

Low-temperature fabrication of boron-doped amorphous silicon passivating contact as a local selective emitter for high-efficiency *n*-type TOPCon solar cells



Hongliang Yu^{a,c}, Wei Liu^a, Haojiang Du^{a,c}, Zunke Liu^{a,c}, Mingdun Liao^a, Ning Song^d, Zhenhai Yang^{a,b,*}, Yuheng Zeng^{a, **}, Jichun Ye^{a,c}

^a Zhejiang Provincial Engineering Research Center of Energy Optoelectronic Materials and Devices, Ningbo Institute of Materials Technology and Engineering, Chinese Academy of Sciences (CAS), Ningbo 315201, China

^b School of Optoelectronic Science and Engineering and Collaborative Innovation Center of Suzhou Nano Science and Technology, Key Lab of Advanced Optical Manufacturing Technologies of Jiangsu Province and Key Lab of Modern Optical Technologies of Education Ministry of China, Soochow University, Suzhou 215006, China

^c University of Chinese Academy of Sciences, Beijing 100049, China

^d School of Photovoltaics and Renewable Energy Engineering, University of New South Wales, Australia

ARTICLE INFO

Keywords:

TOPCon
Boron emitters
Low temperature
Amorphous silicon
Contact resistance

ABSTRACT

Tunnel oxide passivating contact (TOPCon) solar cells (SCs) currently dominate the photovoltaic industry but grapple with efficiency challenges. A primary concern is the direct contact between front-sided metal electrodes and boron emitters, resulting in substantial carrier recombination losses and limiting further efficiency improvements. Here, we introduce a low-temperature approach to deposit a local boron-doped amorphous silicon [a-Si:H(p)] between front-sided metal electrodes and boron emitters. This method, avoiding issues associated with high-temperature processes, demonstrates excellent passivation and contact properties, featuring the lowest contact resistivity ($< 1 \text{ m}\Omega\text{-cm}^2$) and a low saturation current density ($< 400 \text{ fA/cm}^2$). The outstanding passivation and contact properties remain robust even with variations in diborane flow rates during a-Si:H(p) fabrication, annealing temperatures, and sheet resistances of boron emitters. We elucidate the factors contributing to the enhanced passivation observed in boron emitters with a-Si:H(p) through a combination of simulations and experiments. The a-Si:H(p) layer between boron emitters and metal electrodes acts as a protective barrier, preventing the diffusion of metal atoms and suppressing carrier recombination. A heterojunction is formed between a-Si:H(p) and the boron emitter, facilitating electric-field passivation. Consequently, the TOPCon SCs incorporating a-Si:H(p) achieve an efficiency of 24.50%, surpassing their counterparts without a-Si:H(p) (23.11%). This work utilizes low-temperature technology to achieve fully passivated contact, providing insights for the development of high-efficiency TOPCon SCs.

1. Introduction

Tunnel oxide passivating contact (TOPCon) solar cells (SCs) have emerged as the mainstream photovoltaic (PV) technology, owing to their notable advantages of high power conversion efficiency (PCE) and cost-effectiveness in mass production [1–3]. Continuous advancements in efficiency and cost reduction are crucial for promoting the competitiveness of TOPCon SCs in the PV industry. Rigorous numerical

simulations indicate that TOPCon SCs, with optimal passivation and contact properties, can achieve a theoretical efficiency of 28.7%, making them the most promising technology to approach the efficiency limit of crystalline silicon (c-Si) SCs (29.4%) [4,5]. However, further improving the efficiency of TOPCon SCs remains challenges due to inherent limitations in surface passivation and contact resistance. In a typical high-efficiency TOPCon SCs, over 60% of the recombination loss occurs on the front side, whereas less than 25% recombination loss is attributed

* Corresponding author at: Zhejiang Provincial Engineering Research Center of Energy Optoelectronic Materials and Devices, Ningbo Institute of Materials Technology and Engineering, Chinese Academy of Sciences (CAS), Ningbo 315201, China

** Corresponding authors.

E-mail addresses: yangzhenhai@nimte.ac.cn (Z. Yang), yuhengzeng@nimte.ac.cn (Y. Zeng), jichun.ye@nimte.ac.cn (J. Ye).

to the rear side, owing to the excellent passivation and contact properties of the c-Si/SiO₂/poly-Si(*n*⁺) stack [6]. Despite improvements in silicon wafer quality, reduction in the thickness of c-Si wafers, and optimization efforts on the rear-sided TOPCon, resulting in low front- and rear-sided saturation current densities (*i.e.*, $J_{0,\text{pass}}$ and $J_{0,\text{rear}}$) of less than 1 and 5 fA/cm², respectively [7–9], substantial improvements in efficiency are still challenging. The primary challenge lies in addressing significant recombination losses in the boron emitter, where the low boron concentration in the boron emitter/metal contact region hinders further reduction in recombination losses at the metal/silicon interface. For instance, if the saturation current densities of the front metal/emitter interface ($J_{0,\text{met}}$) and the uncontacted interface (*i.e.*, $J_{0,\text{pass}}$) are 600–800 and 8–12 fA/cm², respectively, even with only a 1.5%–2.0% metallization fraction, it results in the saturation current densities of the front metal/emitter ($J_{0,\text{e}}$) reaching 17–28 fA/cm² [10]. This limitation severely impedes improvements in the open-circuit voltage (V_{oc}) and efficiency, especially on the boron emitters with high sheet resistivity (R_{sheet}) that are currently widely used. Another substantial challenge is the high contact resistivity of boron-doped emitters, possibly due to excessive Schottky barriers caused by Fermi energy level pinning effect [11,12], especially when the surface boron concentration is lower than 10¹⁹ cm^{−3} with a sheet resistance of > 150 Ω/sq, which will result in high contact resistance and thus severely limit the fill factor (FF) of TOPCon SCs. Therefore, the carrier recombination loss at the front-sided metal/boron emitter interface, controlled by passivation quality and contact resistivity, presents the most significant bottleneck to efficiency improvement of TOPCon SCs [13–16].

To address these limitations, the technology of laser doping selective emitters has been widely explored [17,18]. This approach aims to improve the contact performance of the contact region by employing lasers to increase the doping concentration of the boron emitter below metal fingers. However, this method cannot avoid direct contact of metal electrodes with boron emitters, and consequently, it fails to essentially inhibit carrier recombination loss of the electrode interface [19,20]. As a promising alternative technology, poly-finger presents an opportunity to achieve fully passivating contact by forming a full-area poly-Si layer on boron emitters and selectively etching of the poly-Si film in the uncontacted region to form a poly-Si selective contact [8, 21]. Currently, the $J_{0,\text{met}}$ and contact resistivity of boron emitters with poly-finger can be reduced to less than 20 fA/cm² and 2 mΩ·cm², respectively [8,22]. However, this technique has limitations as it involves laser pre-opening and high-temperature annealing (over 800°C) to form poly-Si, making it more challenging to selectively etch poly-Si film in the uncontacted region [23,24]. Additionally, the crystallization process of poly-Si during high-temperature treatment may alter the boron and phosphorus diffusion profiles of the front-sided emitters and rear-sided TOPCon structure, respectively. Therefore, the development of a low-temperature process for achieving full passivation contact is critical for further promoting the efficiency of TOPCon SCs.

In this work, we develop a low-temperature process (< 200°C) for creating selective boron emitters through the local deposition of boron-doped amorphous silicon [a-Si:H(p)]. This approach avoids direct contact between the metal electrodes and the boron emitter, resulting in improved passivation and contact properties. By optimizing the a-Si:H(p) fabrication process and annealing conditions, the lowest contact resistivity (< 1 mΩ·cm²) between the metal electrodes and the boron emitters, together with a low $J_{0,\text{met}}$ (< 400 fA/cm²), can be achieved. The superior passivation and contact properties can be well-maintained even under various diborane flow rates for a-Si:H(p) fabrication, annealing temperatures, and sheet resistances of boron emitters. We elucidate the factors contributing to the enhanced passivation performance observed in boron emitters with a-Si:H(p) through a combination of simulations and experiments. The a-Si:H(p) layer between boron emitters and metal electrodes acts as a protective barrier, preventing the diffusion of metal atoms and suppressing carrier recombination. The presence of a-Si:H(p) can form a heterojunction when combined with a

boron emitter, thereby promoting electric-field passivation. Consequently, the TOPCon SCs incorporating a-Si:H(p) achieve a PCE of 24.50%, outperforming their counterparts without a-Si:H(p) (23.11%).

2. Experimental details

The substrates used for characterization were *n*-type CZ wafers with a <100> orientation, a thickness of 165 μm, and a resistivity of 1–3 Ω·cm. The front- and rear-sided silicon wafers were textured by KOH etching. Following RCA cleaning and diluted HF immersion, a high-temperature BBr₃ diffusion process was employed to form double-sided boron-doped emitters with a R_{sheet} of 108–240 Ω/sq. The a-Si:H(p) films were deposited using a PECVD system operating at a frequency of 13.56 MHz, a deposition temperature of 150°C, and employing SiH₄, H₂, and diborane (B₂H₆) as precursors. The boron diffusion profiles were adjusted by controlling the B₂H₆ flow rate. Subsequently, a 10 nm-thick silver layer was thermally evaporated on the a-Si:H(p) films for $J_{0,\text{met}}$ measurements [25,26].

The manufacturing process for TOPCon SCs is described below. Silicon wafers were textured by etching with a KOH alkaline solution. Front-sided boron emitters were formed using the high-temperature BBr₃ diffusion method, and rear-sided boron-doped poly-Si films underwent HNO₃-HF-H₂ acid polishing. Silicon oxide film was fabricated by oxidation in a tube furnace at 100°C in an ozone atmosphere, followed by PECVD deposition of phosphorus-doped a-Si:H using silane, phosphane and H₂ as precursors. High-temperature annealing at 840°C was carried out in a quartz tube furnace under a nitrogen atmosphere to achieve a-Si:H crystallization and dopant diffusion. The samples were covered by ALD-deposited AlO_x passivation layers and activated through annealing at 450°C. Subsequently, samples were covered with PECVD-deposited SiN_x layers on both sides. The front-sided finger electrode mask with a line width of 6 μm was defined using photolithography. The SiN_x and AlO_x films upon the fingers were etched using a buffered oxide etch (BOE) solution, and a-Si:H(p) film was deposited by PECVD. A Ni/Pd/Ag seed layer was deposited by electron beam evaporation, followed by forming gas anneal (FGA) at 400°C for 30 min, and the electrode thickness is increased to 5 μm. After that, the rear-sided Cr-Ag electrode was deposited by thermal evaporation.

Microstructure of the a-Si:H(p) film, together with corresponding elemental distributions, was studied using a scanning electron microscope (SEM) (Hitachi, S4800) and high resolution transmission electron microscope (HR-TEM) (ThermoFisher, Talos F200 X). R_{sheet} was measured using a four-point probe meter (Polytec, Four Dimensions). Contact resistivity was measured using a semiconductor parameter analyzer (Keithley 4200-SCS) combined with the transfer length method (TLM) [27]. The TLM template employs eight rectangular metal electrodes with a length (L) of 0.5 cm and a width (W) of 0.1 cm arranged in a linear pattern. The distribution profiles of activated boron atoms at the emitter were measured using an electrochemical capacitive voltage (ECV) system (Buchanan, CVP 21). Passivation parameters were analyzed by a quasi-steady-state photoconductance (QSSPC, Sinton WCT-120). The implied open-circuit voltage (iV_{oc}) of the samples after metallization was extracted using photoluminescence spectroscopy (PL) (Ai-Shine, Suns-EPL) with a shutter parameter of 1500, where the side covering the metal electrode faces the light source. The electrical performance of TOPCon SCs was characterized by the Suns- V_{oc} analysis system (Sinton WTC-120) under a sun simulator (Enlitech, SS-F5-3A) at 25°C and AM 1.5 G (100 mW·cm^{−2}). External quantum efficiency (EQE) spectra of TOPCon SCs were measured using the EQE system (Enlitech, QE-R3011).

3. Results and discussion

3.1. Fabrication and characterization of boron emitters with a-Si:H(p)

The schematic diagrams in Fig. 1A illustrate the fabrication process

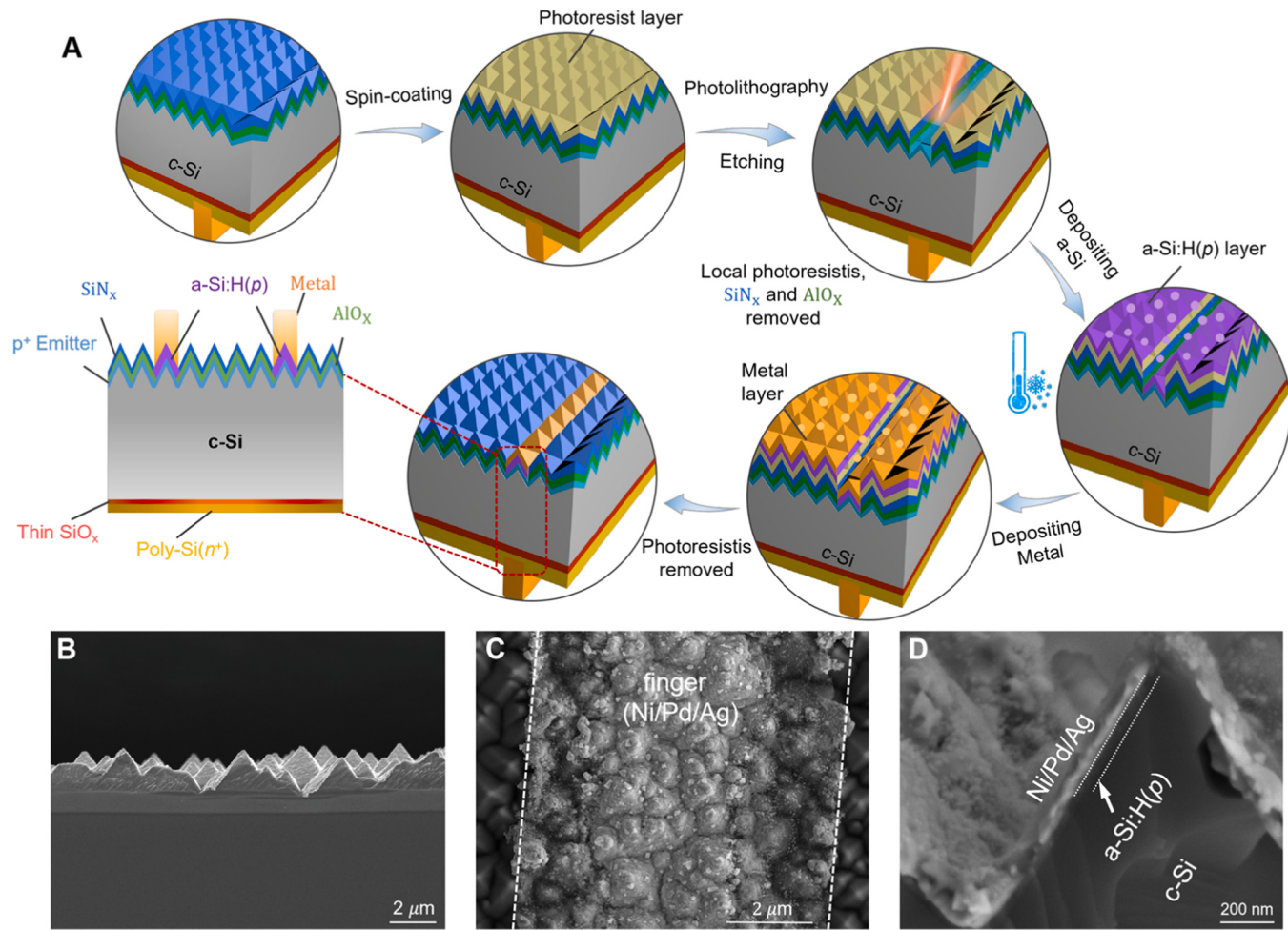


Fig. 1. (A) Schematic diagrams describing the fabrication process of TOPCon SCs with a local a-Si:H(p) passivating contact. SEM images of (B) the cross-section of device based on a-Si:H(p), (C) front-sided finger, and (D) a local SEM image of device with an a-Si:H(p) structure, showing a remarkable interlayer between the metal stack and the c-Si substrate.

of TOPCon SCs with a local a-Si:H(p) passivation contact underneath the front-sided metal fingers. A semi-finished TOPCon SCs with the passivation layer and the anti-reflective coating (ARC) layers (i.e., AlO_x/SiN_x stack) was prepared in advance, and then photoresist was applied to the front side of the samples for accurate patterning. The AlO_x/SiN_x stack underneath the electrode pattern was selectively etched away, and a 30–40 nm-thick a-Si:H(p) film was deposited at a low temperature of 150°C using PECVD, followed by the direct deposition of a metal electrode using an electron beam system. After removing the photoresist, an FGA process at 400°C for 30 min was carried out. Finally, the front-sided busbars and rear-sided electrodes were deposited to complete the fabrication of TOPCon SCs.

Observing the morphology of the devices under a SEM, as shown in Fig. 1B–1D, the pyramid structure of locally deposited a-Si:H(p) with the metal stack is well-formed. The width of the metal fingers is slightly larger than the photolithography line (6 μm), but it uniformly covers the surface of the pyramids. A local view of the cross-sectional SEM image in Fig. 1C reveals the a-Si:H(p) layer covering the substrate with good contact between the Ni/Pd/Ag electrode and the a-Si:H(p). These SEM images demonstrate the integrity and manufacturability of the TOPCon SCs based on a local a-Si:H(p) underneath the front-sided metal fingers.

3.2. Contact properties of boron emitter with a-Si:H(p)

The activated boron concentration significantly influences the conductivity of a-Si:H(p) films, which will be investigated in this section.

Here, the fixed hydrogen dilution ratio (H₂:SiH_x) was maintained at 20:3 (in sccm, denoting cubic centimeter per minute at stand temperature and pressure). Subsequently, 40 nm-thick a-Si:H(p) films with different diborane flow rates were deposited on symmetrical boron emitters at a low temperature of 150°C using PECVD, followed by an FGA process at 400°C for 30 min. ECV measurements were employed to determine the profiles of the activated boron concentration, as shown in Fig. 2A and 2B. Fig. 2A exhibits that the activated boron concentration within the emitter and c-Si substrate, as well as the activated boron depth in the c-Si substrate, increase with the diborane flow rate, which is higher than that of the counterpart with the boron emitter without a-Si:H(p). Additionally, the surface concentration of activated boron for a diborane flow rate of 10 sccm, as shown in Fig. 2B, increases significantly by an order of magnitude compared to the case without a-Si:H(p), effectively addressing the low doping concentration challenge of the laser selective emitter technique [28].

Contact resistivities of these samples are measured using the TLM method (Figures S1 and S2). Samples were prepared by depositing a Ni/Pd/Ag stack upon the emitter, followed by an FGA process at 400°C for 30 min. Fig. 2C illustrates the variation of contact resistivity with the diborane flow rate. With the flow rate of diborane increasing from 3 to 10 sccm, the contact resistivity decreases from 6.3 to 1.0 mΩ·cm², indicating a substantial improvement in contact property compared to the boron emitter without a-Si:H(p) (24.3 mΩ·cm²). This finding is consistent with the ECV results, suggesting that a high diborane flow rate results in a high surface activated boron concentration and improved

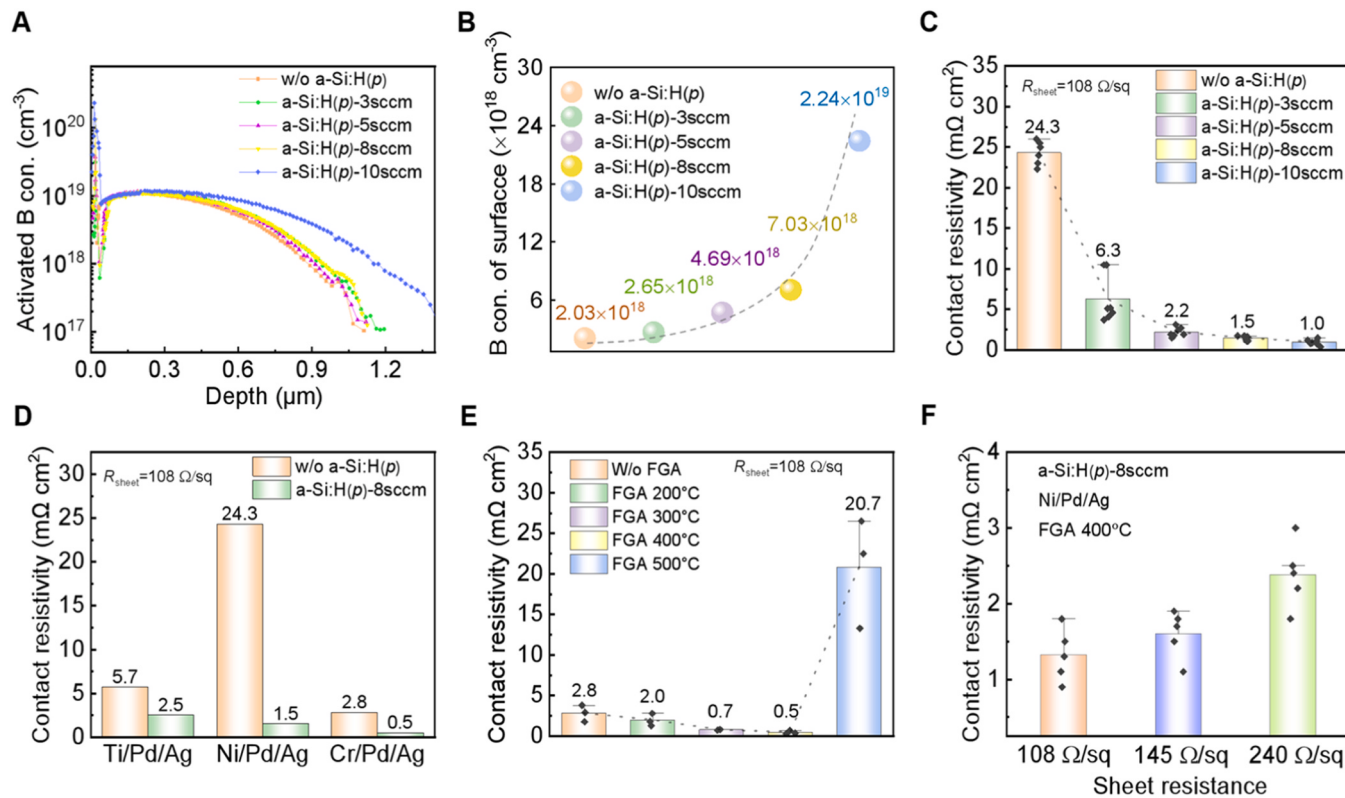


Fig. 2. (A) Activated B profiles, and (B) the corresponding surface boron concentrations under different diborane flow rates measured by ECV. Contact resistivity of samples under the different (C) diborane flow rates, (D) metal electrodes, (E) FGA temperatures, and (F) sheet resistances.

electrical conductivity [29]. The various metal materials are studied to investigate their effect on electrical properties, as shown in Fig. 2D. The contact resistivities of samples with a-Si:H(p) covered by Ti/Pt/Ag, Ni/Pt/Ag, and Cr/Pt/Ag stacks are determined to be 2.5, 1.5, and 0.5 $\text{m}\Omega \cdot \text{cm}^2$, respectively, much lower than those of samples without a-Si:H(p), i.e., 5.7, 24.3, and 2.8 $\text{m}\Omega \cdot \text{cm}^2$ for the three related cases. This implies that the introduction of a-Si:H(p) layers underneath the front-sided metal fingers can significantly improve contact properties, regardless of the metal materials used. Furthermore, the Cr/Pt/Ag stack has lowest contact resistivity, possibly due to the relatively high work-function of Cr [30,31].

The impact of FGA temperature on the contact properties is also investigated, as demonstrated in Fig. 2E. For FGA temperatures lower than 200°C, annealing has no noticeable effect on contact resistivity. With the FGA temperature increasing from 200°C to 400°C, the contact resistivity shows a slight decreasing trend, indicating that a low-temperature FGA process (< 500°C) leads to a significant improvement in contact properties. However, at the FGA temperature of 500°C, the contact resistivity significantly increases to over 20 $\text{m}\Omega \cdot \text{cm}^2$. It is speculated that low-temperature annealing (< 500°C) may form a metal silicide at the interface, reducing contact resistivity, while high-temperature annealing may damage the interface layer between metal fingers and boron emitters, leading to an increase in contact resistivity [30]. To ensure compatibility between the a-Si:H(p) layer and high sheet resistance emitters currently used in the industry, a-Si:H(p) layers were deposited on boron emitters featuring varying sheet resistances. Fig. 2F and S3 show that the contact resistivity can be well-maintained at relatively low values, and no significant variation in the contact resistivity values is observed, suggesting that the introduction of the a-Si:H(p) layer can achieve low contact resistivity even for the boron emitters with high sheet resistances.

3.3. Passivation properties and mechanism of boron emitters with a-Si:H(p)

In this section, passivation properties of boron emitters with a-Si:H(p) will be investigated. The structure used for passivation measurement is illustrated in Fig. 3A, where a-Si:H(p) films were deposited on both sides of boron emitters. Fig. 3A depicts an increase in recombination current from 40 to 305 fA/cm^2 after the deposition of double-sided a-Si:H(p) on the boron emitters. The passivation quality of samples with a-Si:H(p) significantly decreases compared to the pristine boron emitter without a-Si:H(p). This is a result of the presence of a boron-enriched a-Si:H layer with a high doping concentration and epitaxial growth of the a-Si:H layer occurring at a low PECVD frequency, which together result in high carrier recombination losses [32]. Reduced boron diffusion with high sheet resistance is recognized to reduce Auger recombination, evaluated by $J_{0,e}$. However, as the sheet resistance increases, the contact and lateral resistance increase, leading to the decrement in filling factor (FF) of devices [33]. The contact recombination between a-Si:H(p) and metal electrodes is the focus of this study. After metallization, the recombination current density in the metal-contact region is determined to be 360 fA/cm^2 . While there exists a slight rise in recombination current density concerning pre-metallization, it is still nearly 300 fA/cm^2 lower than the samples without a-Si:H(p) (730 fA/cm^2).

In order to enhance the passivation performance, we monitor the passivation before metallization, and firstly prepared a semi-finished TOPCon device without front- and rear-sided electrodes, which were passivated with an $\text{AlO}_x/\text{SiN}_x$ stack, exhibiting an implied open-circuit voltage of 730 mV and a $J_{0,e}$ of 10 fA/cm^2 . After metallization, the samples without a-Si:H(p) appear noticeably darker in the vicinity of the metal fingers, as shown by the PL images in Fig. 3C. This suggests that the metal atoms have already diffused into the boron emitters to form recombination centers during metallization, ultimately resulting in a degradation of the passivation performance. After deriving the

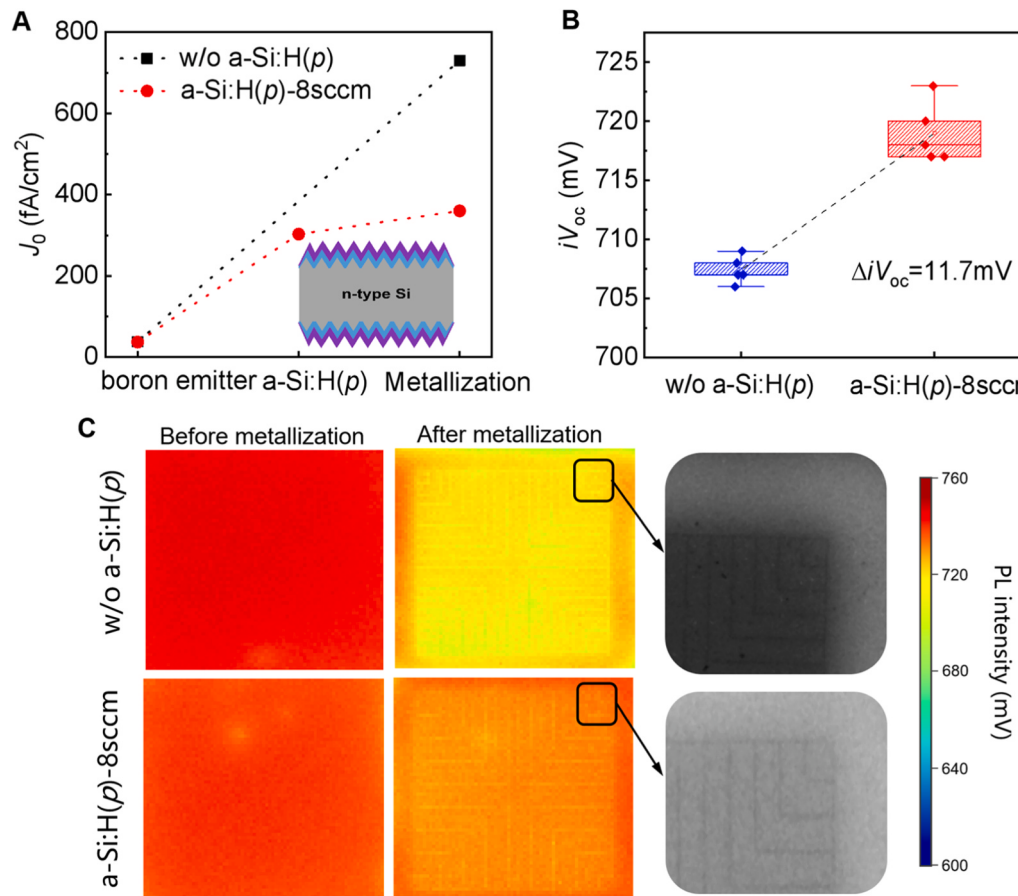


Fig. 3. (A) J_0 and (B) iV_{oc} of samples with and without a-Si:H(p) after metallization. (C) PL images of samples with and without a-Si:H(p) before and after metallization.

corresponding iV_{oc} with parameter correction using PL, it can be clearly seen that the iV_{oc} of the samples with a-Si:H(p) is improved by 11.7 mV compared to the counterpart without a-Si:H(p), significantly improving the passivation properties after metallization (Fig. 3B).

The improved passivation quality may be attributed to the a-Si:H(p) layer acting as a buffer layer, preventing the diffusion of metal atoms into the boron emitters and thereby reducing carrier recombination losses [34]. Additionally, a heterojunction formed by a-Si:H(p) and the boron emitter proves advantageous for energy bending, enhancing electric-field passivation, and mitigating carrier recombination [35]. To validate these hypotheses, TEM and energy dispersive spectroscopy (EDS) measurements were conducted, where full-area Ni/Pd/Ag metal electrodes were deposited on the boron emitters. The results in Fig. 4A reveals that, for samples without a-Si:H(p), a distinct Ag signal within the boron emitter is observed, indicating the diffusion of Ag atoms into the boron emitter. In contrast, samples with a-Si:H(p) exhibit a relatively lower Ag signal within the boron emitters, suggesting suppressed Ag diffusion with the introduction of a-Si:H(p) between metal electrodes and boron emitters. For visual comparison, the atom fractions are plotted in Fig. 4C, S4 and S5, indicating Ag atom fractions within boron emitter region of 31.3% and 4.2% for the samples without and with a-Si:H(p), respectively. Furthermore, the results in Fig. 4C also demonstrate that the distribution of Ni and Pd for samples with a-Si:H(p) is more concentrated, indicating suppressed metal atom diffusion [36]. To further illustrate the impact of a-Si:H(p) on passivation performance, energy band diagrams for the cases with and without a-Si:H(p), calculated based on the doping profiles obtained from ECV curves in Fig. 2A, are presented in Fig. 4D. It is evident from Fig. 4D that a heterojunction between a-Si:H(p) and the boron emitter is formed, attributed to enhance interface electric-field intensity and hinder minority carrier

recombination, thereby improving passivation quality.

3.4. Performance of TOPCon SCs with a-Si:H(p)

In the last section, we construct a proof-of-concept TOPCon SC with a boron-emitter R_{sheet} of $\sim 150\ \Omega/\text{sq}$ to illustrate the advantages of a-Si:H(p) as a local passivating contact for boron emitters, providing further validation for the feasibility of employing this method in the fabrication of boron emitters for TOPCon SCs. The schematic structure of the TOPCon SCs featuring a-Si:H(p) is depicted in Fig. 5A. As shown in Fig. 5B, the TOPCon structures, featuring Ni/Pd/Ag metal stack and a-Si:H(p) with B_2H_6 of 8 sccm and FGA at 400°C for 30 min, demonstrate an effective lifetime of 2.32 ms at $\Delta n = 10^{15}\ \text{cm}^{-3}$ and a remarkable implied fill factor (iFF) of 85.43%, higher than that of the counterpart without a-Si:H(p), i.e., an effective lifetime of 1.43 ms at $\Delta n = 10^{15}\ \text{cm}^{-3}$ and an iFF of 82.33%.

The $J-V$ curves of the TOPCon SCs without and with a-Si:H(p) are plotted in Fig. 5C, where the detailed electrical parameters of the two related cases are tabulated in the inset. TOPCon SCs with a-Si:H(p) demonstrate an optimal efficiency of 24.50%, a V_{oc} of 696 mV, a J_{sc} of 42.03 mA·cm⁻², and an FF of 83.76%. In contrast, TOPCon SCs without a-Si:H(p) receive an efficiency of 23.11%, a V_{oc} of 689 mV, a J_{sc} of 41.80 mA·cm⁻², and an FF of 80.39%. The improvements in V_{oc} and FF suggest improved passivation and contact properties. The corresponding external quantum efficiency (EQE) spectra are demonstrated in Fig. 5D, which shows that TOPCon SCs with a-Si:H(p) exhibit a slightly increased EQE, especially in the short-wavelengths. It is noting that the V_{oc} values obtained from the $J-V$ curves are lower than the voltages obtained after the front-sided metallization, owing to losses during both the front- and rear-sided metallization of busbars (Figure S6), which is an issue that

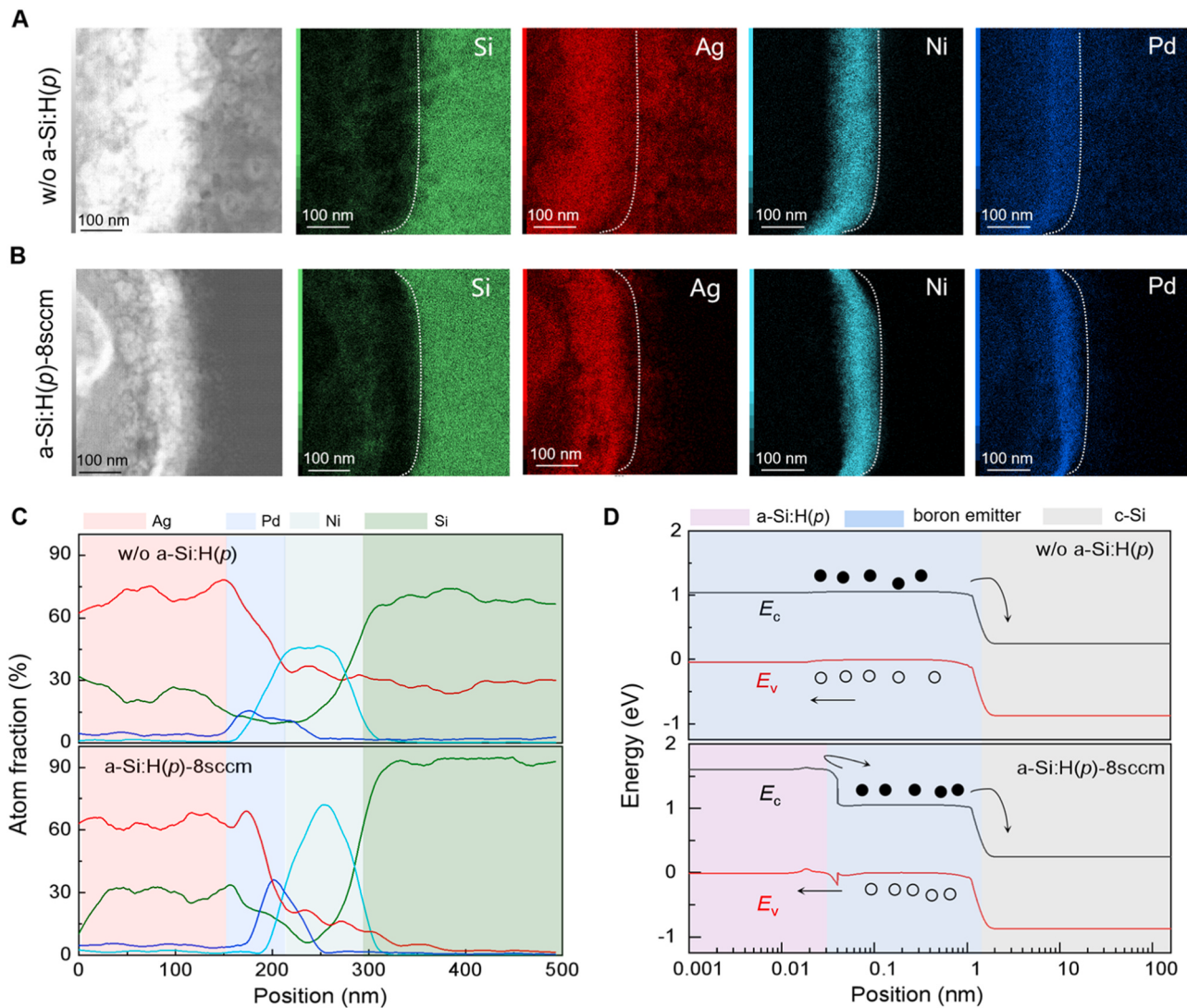


Fig. 4. Cross-sectional TEM images and the corresponding EDS mappings of Si, Ag, Ni, and Pd elements of samples (A) without and (B) with a-Si:H(p). (C) Atom fraction plots extracted from Fig. 4A and 4B for the two related samples. (D) Energy band diagrams for the two related cases, which were obtained by extracting the doping profiles from ECV.

needs to be addressed.

4. Conclusion

In this work, we presented a low-temperature method for achieving selective boron emitters using PECVD deposition of a-Si:H(p) between boron emitters and metal electrodes, resulting in improved passivation and contact properties. Through the optimization of the fabrication process of a-Si:H(p) and annealing conditions, we successfully achieved a low contact resistivity of less than $1 \text{ m}\Omega\cdot\text{cm}^2$ between the metal electrodes and the boron emitters, as well as a low $J_{0,\text{met}}$ of less than 400 fA/cm^2 . Additionally, excellent passivation and contact properties were maintained under various diborane flow rates for a-Si:H(p) fabrication, annealing temperatures, and sheet resistances of boron emitters, highlighting the robustness of a-Si:H(p) in achieving high passivation and contact properties. Mechanisms contributing to the improved passivation quality of boron emitters covered by a-Si:H(p) were elucidated through simulations and experiments. The presence of the a-Si:H(p) layer between boron emitters and metal electrodes serves as a buffer layer, preventing the diffusion of metal atoms and suppressing carrier recombination. A heterojunction formed by a-Si:H(p) and the boron emitter is favorable for promoting energy band bending, providing

strengthened electric-field passivation. As a result, the TOPCon SCs with a boron-emitter R_{sheet} of $\sim 150 \text{ }\Omega/\text{sq}$ utilizing a-Si:H(p) after metallization received an average iV_{oc} of 718 mV and a PCE of 24.50%, surpassing the counterpart without a-Si:H(p) with an iV_{oc} of 707 mV and a PCE of 23.11%.

This work presents an advanced approach to prepare selective boron emitters based on a-Si:H(p), featuring a complete low-temperature process that is compatible with photoresist. This simplified process has the potential to be compatible with electroplating processes in the future. By carefully controlling the a-Si:H(p) layer, metal stacks, and annealing conditions, excellent contact properties with low contact resistivity and high passivation with low $J_{0,\text{met}}$ were achieved. Importantly, this approach is fully compatible with boron emitters with high sheet resistance, providing a viable solution to enhance the efficiency of TOPCon SCs.

CRediT authorship contribution statement

Hongliang Yu: Writing – original draft, Software, Methodology, Investigation, Formal analysis, Data curation, Conceptualization. **Yuheng Zeng:** Writing – review & editing, Supervision, Project administration, Investigation, Funding acquisition, Data curation,

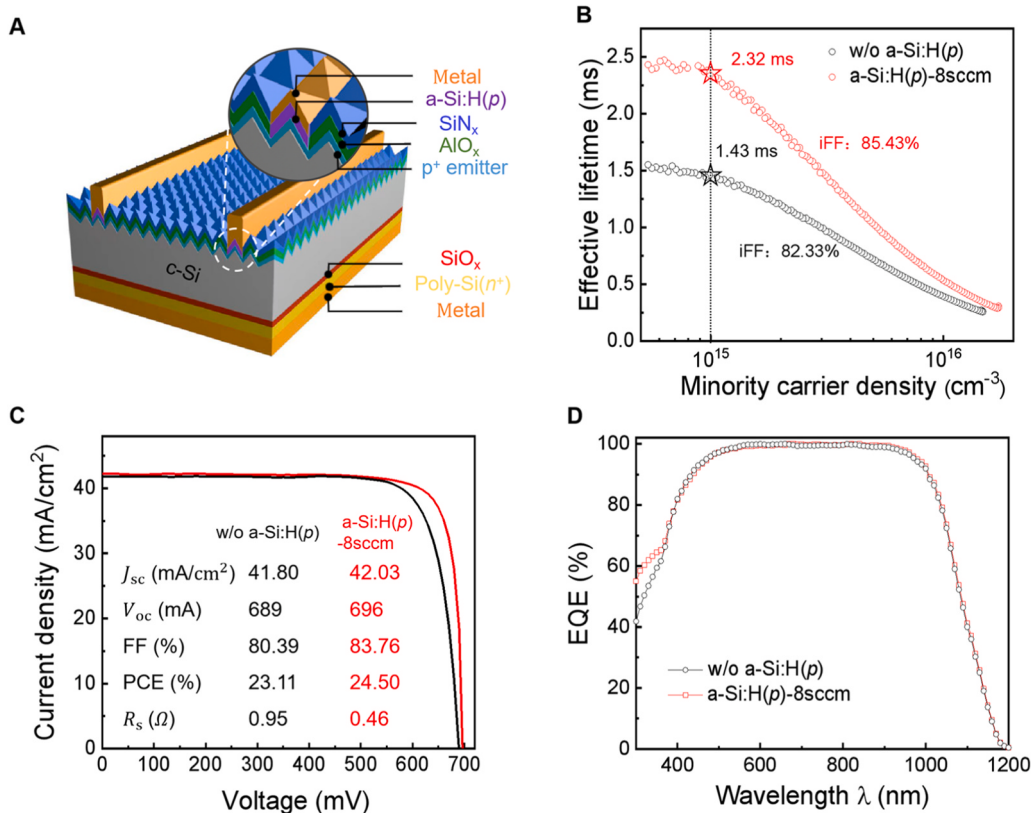


Fig. 5. (A) Schematic diagram of TOPCon SCs featuring a-Si:H(p). (B) Effective lifetime curves as a function of minority carrier density (Δn) for the TOPCon SCs without and with a-Si:H(p). (C) J-V characteristic curves, and (D) the corresponding EQE curves of the two related TOPCon SCs, where the electrical parameters are inserted in Fig. 5C. The R_{sheet} of the boron-emitter used for the SCs is $\sim 150 \Omega/\text{sq}$.

Conceptualization. Ning Song: Conceptualization, Formal analysis. Zhenhai Yang: Writing – review & editing, Supervision, Project administration, Investigation, Formal analysis, Data curation, Conceptualization. Jichun Ye: Writing – review & editing, Data curation. Haojiang Du: Investigation, Formal analysis, Data curation. Wei Liu: Investigation, Formal analysis, Data curation. Mingdun Liao: Data curation. Zunke Liu: Data curation.

Declaration of Competing Interest

The authors declare that they have no known competing financial interests or personal relationships that could have appeared to influence the work reported in this paper.

Data availability

Data will be made available on request.

Acknowledgements

This work was supported by the Ningbo “Innovation 2025” Major Project (2022Z114, 2020Z098), the National Natural Science Foundation of China (61974178, 61874177), the Key Research and Development Program of Zhejiang Province (2021C01006), the National Key R&D Program of China (Grant No. 2018YFB1500403), the Youth Innovation Promotion Association (2018333), the Zhejiang Provincial Natural Science Foundation (LY19F040002), Science and technology projects in Liaoning Province 2021 (2021JHI/10400104), the Key Research and Development Program of Zhejiang Province (2024C01055).

Appendix A. Supporting information

Supplementary data associated with this article can be found in the online version at [doi:10.1016/j.nanoen.2024.109556](https://doi.org/10.1016/j.nanoen.2024.109556).

References

- Glunz S.W., Hermle M., Reichel C., Bivour M., Feldmann F., A. Passivated Rear Contact for High-Efficiency n-Type Si Solar Cells Enabling High V_{oc} 's and FF > 82%, 28th European PV Solar Energy Conference and Exhibition, 2013.
- F. Feldmann, M. Bivour, C. Reichel, M. Hermle, S.W. Glunz, Passivated rear contacts for high-efficiency n-type Si solar cells providing high interface passivation quality and excellent transport characteristics, Sol. Energy Mater. Sol. Cells 120 (2014) 270–274, <https://doi.org/10.1016/j.solmat.2013.09.017>.
- F. Feldmann, M. Bivour, C. Reichel, H. Steinkemper, M. Hermle, S.W. Glunz, Tunnel oxide passivated contacts as an alternative to partial rear contacts, Sol. Energy Mater. Sol. Cells 131 (2014) 46–50, <https://doi.org/10.1016/j.solmat.2014.06.015>.
- A. Richter, M. Hermle, S.W. Glunz, Reassessment of the limiting efficiency for crystalline silicon solar cells, IEEE J. Photovolt. 3 (4) (2013) 1184–1191, <https://doi.org/10.1109/JPHOTOV.2013.2270351>.
- R. Peibst, M. Rienäcker, Y. Larionova, N. Folchert, F. Haase, C. Hollemann, S. Wolter, J. Krüger, P. Bayerl, J. Bayer, M. Dzinnik, R.J. Haug, R. Brendel, Towards 28%-efficient Si single-junction solar cells with better passivating POLO junctions and photonic crystals, Sol. Energy Mater. Sol. Cells 238 (2022) 111560, <https://doi.org/10.1016/j.solmat.2021.111560>.
- S. Glunz, F. Feldmann, A. Richter, M. Bivour, C. Reichel, H. Steinkemper, J. Benick, M. Hermle, The irresistible charm of a simple current flow pattern – 25% with a solar cell featuring a full-area back contact (2015) <https://doi.org/10.4229/EUPVSEC2015-2BP.1.1>.
- D. Chen, Y. Chen, Z. Wang, J. Gong, C. Liu, Y. Zou, Y. He, Y. Wang, L. Yuan, W. Lin, R. Xia, L. Yin, X. Zhang, G. Xu, Y. Yang, H. Shen, Z. Feng, P.P. Altermatt, P. J. Verlinden, 24.58% total area efficiency of screen-printed, large area industrial silicon solar cells with the tunnel oxide passivated contacts (i-TOPCon) design, Sol. Energy Mater. Sol. Cells 206 (2020) 110258, <https://doi.org/10.1016/j.solmat.2019.110258>.
- P. Padhamnath, J. Wong, B. Nagarajan, J.K. Batis, L.M. Ortega, N. Nandakumar, A. Khanna, V. Shanmugam, S. Duttagupta, Metal contact recombination in monoPoly™ solar cells with screen-printed & fire-through contacts, Sol. Energy

- Mater. Sol. Cells 192 (2019) 109–116, <https://doi.org/10.1016/j.solmat.2018.12.026>.
- [9] Z. Liu, Z. Lin, W. Liu, L. Yang, N. Lin, M. Liao, X. Yu, Z. Yang, Y. Zeng, J. Ye, Regionalizing nitrogen doping of polysilicon films enabling high-efficiency tunnel oxide passivating contact silicon solar cells, *Small* 19 (49) (2023) 2304348, <https://doi.org/10.1002/smll.202304348>.
- [10] M.S. Jeong, K.H. Min, S. Choi, M.G. Kang, K.T. Jeong, E.T. Lee, Y. Kang, D. Kim, H.-S. Lee, H.-E. Song, S. Park, Correlation between the open-circuit voltage and recombination loss at metal-silicon interfaces of crystalline silicon solar cells, *Sol. Energy Mater. Sol. Cells* 210 (2020) 110519, <https://doi.org/10.1016/j.solmat.2020.110519>.
- [11] T.G. Allen, J. Bullock, X. Yang, A. Javey, S. De Wolf, Passivating contacts for crystalline silicon solar cells, *Nat. Energy* 4 (11) (2019) 914–928, <https://doi.org/10.1038/s41560-019-0463-6>.
- [12] J. Melskens, B.W.H. v.d. Loo, B. Macco, L.E. Black, S. Smit, W.M.M. Kessels, Passivating contacts for crystalline silicon solar cells: from concepts and materials to prospects, *IEEE J. Photolt.* 8 (2) (2018) 373–388, <https://doi.org/10.1109/JPHOTOV.2018.2797106>.
- [13] M.K. Stodolny, M. Lenes, Y. Wu, G.J.M. Janssen, I.G. Romijn, J.R.M. Luchies, L. J. Gearligs, n-Type polysilicon passivating contact for industrial bifacial n-type solar cells, *Sol. Energy Mater. Sol. Cells* 158 (2016) 24–28, <https://doi.org/10.1016/j.solmat.2016.06.034>.
- [14] N. Wöhrle, E. Lohmüller, J. Greulich, S. Werner, S. Mack, Towards understanding the characteristics of Ag-Al spiking on boron-doped silicon for solar cells, *Sol. Energy Mater. Sol. Cells* 146 (2016) 72–79, <https://doi.org/10.1016/j.solmat.2015.11.032>.
- [15] R. Lago, L. Perez, H. Kerp, I. Freire, I. Hoces, N. Azkona, F. Recart, J.C. Jimeno, Screen printing metallization of boron emitters, *Prog. Photovolt.: Res. Appl.* 18 (2010) 20–27, <https://doi.org/10.1002/pip.933>.
- [16] T. Fellmeth, H. Höffler, S. Mack, E. Krassowski, K. Krieg, B. Kafle, J. Greulich, Laser-enhanced contact optimization on i-TOPCon solar cells, *Prog. Photovolt.: Res. Appl.* 30 (2022) 1393–1399, <https://doi.org/10.1002/pip.3598>.
- [17] J. Sungjin, Y. Cha, S. Kim, H. Kim, S. Park, T. Kim, J. Park, M. Ju, J. Yi, Analysis of selective emitter formation technology of n-TOPCon solar cell, *Trans. Korean Inst. Electr. Eng.* 71 (2022) 114–120, <https://doi.org/10.5370/KIEE.2022.71.1.114>.
- [18] G. Poulain, D. Blanc, A. Focsa, B. Bazer-Bachi, M. Gauthier, B. Semmache, Y. Pellegrin, N. Le Quang, M. Lemiti, Laser process for selective emitter silicon solar cells, *Int. J. Photoenergy* 2012 (2012) 413863, <https://doi.org/10.1155/2012/413863>.
- [19] J.M. Yacob Ali, V. Shanmugam, B. Lim, A.G. Aberle, T. Mueller, Femtosecond laser ablation of dielectric layers for high-efficiency silicon wafer solar cells, *Sol. Energy* 164 (2018) 287–291, <https://doi.org/10.1016/j.solener.2018.02.046>.
- [20] C.-Y. Chen, J.-H. Yang, T.-Y. Lin, H.-Y. Ma, I. Chen, Fabrication of local micro-contacts to silicon solar cells by dewetting of ultrathin polymer films, *RSC Adv.* 10 (2020) 5579–5584, <https://doi.org/10.1039/C9RA10457G>.
- [21] M. Xiao, Z. Yang, Z. Liu, H. Du, N. Lin, H. Wei, H. Xing, Q. Wu, W. Liu, M. Liao, B. Yan, Y. Wang, Y. Zeng, J. Ye, SiO_x /polysilicon selective emitter prepared by PECVD-deposited amorphous silicon plus one-step firing enabling excellent $J_{0,\text{met}}$ of $< 235 \text{ fA/cm}^2$ and ρ_c of $< 2 \text{ m}\Omega\text{-cm}^2$, *Sol. Energy* 262 (2023) 111887, <https://doi.org/10.1016/j.solener.2023.111887>.
- [22] A. Chaudhary, J. Hoß, J. Lossen, F. Huster, R. Kopecek, R. van Swaaij, M. Zeman, Influence of polysilicon thickness on properties of screen-printed silver paste metallized silicon oxide/polysilicon passivated contacts, *Phys. Status Solidi A* 218 (18) (2021) 2100243, <https://doi.org/10.1002/pssa.202100243>.
- [23] S.-W. Chang, V.P. Chuang, S.T. Boles, C.V. Thompson, Metal-catalyzed etching of vertically aligned polysilicon and amorphous silicon nanowire arrays by etching direction confinement, *Adv. Funct. Mater.* 20 (24) (2010) 4364–4370, <https://doi.org/10.1002/adfm.201000437>.
- [24] E. Ibok, S. Garg, A characterization of the effect of deposition temperature on polysilicon properties: morphology, dopability, etchability, and polycide properties, *J. Electrochem. Soc.* 140 (10) (1993) 2927, <https://doi.org/10.1149/1.2220934>.
- [25] J. Bullock, D. Yan, Y. Wan, A. Cuevas, B. Demaurex, A. Hessler-Wyser, S. De Wolf, Amorphous silicon passivated contacts for diffused junction silicon solar cells, *J. Appl. Phys.* 115 (16) (2014) 163703, <https://doi.org/10.1063/1.4872262>.
- [26] J. Bullock, A. Cuevas, D. Yan, B. Demaurex, A. Hessler-Wyser, S. De Wolf, Amorphous silicon enhanced metal-insulator-semiconductor contacts for silicon solar cells, *J. Appl. Phys.* 116 (16) (2014) 163706, <https://doi.org/10.1063/1.4900539>.
- [27] H.H. Berger, Contact resistance and contact resistivity, *J. Electrochem. Soc.* 119 (4) (1972) 507, <https://doi.org/10.1149/1.2404240>.
- [28] X. Li, Q. Wang, X. Dong, J. Li, X. Zhang, N. Yuan, L. Li, J. Ding, Optimization of efficiency enhancement of TOPCon cells with boron selective emitter, *Sol. Energy Mater. Sol. Cells* 263 (2023) 112585, <https://doi.org/10.1016/j.solmat.2023.112585>.
- [29] P.A. Tove, Simple dipole model for barrier heights of silicide-silicon and metal-silicon barriers, *Surf. Sci.* 132 (1) (1983) 336–343, [https://doi.org/10.1016/0039-6028\(83\)90546-0](https://doi.org/10.1016/0039-6028(83)90546-0).
- [30] A. Mette, New Concepts for Front Side Metallization of Industrial Silicon Solar Cells, Ph.D thesis, Fraunhofer ISE (2007).
- [31] R.W. Bower, J.W. Mayer, Growth kinetics observed in the formation of metal silicides on silicon, *Appl. Phys. Lett.* 20 (9) (2003) 359–361, <https://doi.org/10.1063/1.1654186>.
- [32] H. Fujiwara, M. Kondo, Impact of epitaxial growth at the heterointerface of a-Si: H/c-Si solar cells, *Appl. Phys. Lett.* 90 (1) (2007) 418, <https://doi.org/10.1063/1.2426900>.
- [33] H. Du, Z. Liu, W. Liu, M. Xiao, N. Lin, W. Yang, Q. Xia, M. Liao, B. Yan, Z. Yang, Y. Zeng, J. Ye, Concurrently preparing front emitter and rear passivating contact via continuous PECVD deposition plus one-step annealing for high-efficiency tunnel oxide passivating contact solar cells, *Sol. RRL* 7 (7) (2023) 2201082, <https://doi.org/10.1002/solr.202201082>.
- [34] S.K. Singh, A.A. Kumbhar, R.O. Dusane, W. Bock, Hot-wire chemical-vapor-deposited nanometer range a-SiCH diffusion barrier films for ultralarge-scale-integrated application, *J. Vac. Sci. Technol. B: Microelectron. Nanometer Struct. Process. Meas. Phenom.* 24 (2) (2006) 543–546, <https://doi.org/10.1116/1.2166862>.
- [35] J. Zheng, Z. Ying, Z. Yang, Z. Lin, H. Wei, L. Chen, X. Yang, Y. Zeng, X. Li, J. Ye, Polycrystalline silicon tunnelling recombination layers for high-efficiency perovskite/tunnel oxide passivating contact tandem solar cells, *Nat. Energy* 8 (11) (2023) 1250–1261, <https://doi.org/10.1038/s41560-023-01382-w>.
- [36] M.A. Nicolet, Diffusion barriers in semiconductor contact technology, *Defect Diffus. Forum* 143–147 (1997) 1271–1284, <https://doi.org/10.4028/www.scientific.net/DDF.143-147.1271>.